Available online at www.sciencedirect.com
SCIENCE DIRECT
Catalysis Today 111 (2006) 103–110
CATALYSIS TODAY
www.elsevier.com/locate/cattod

Four challenges for nickel steam-reforming catalysts

Jens Sehested *

Haldor Topsøe A/S, DK-2800 Lyngby, Denmark

Available online 23 November 2005

Abstract

Reforming over supported nickel catalysts has been used commercially for more than 40 years. In this paper four catalytic challenges for nickel steam reforming catalysts are discussed from both a practical and a fundamental point of view. The four challenges are activity, sulphur poisoning, carbon formation and sintering. A coherent microscopic picture of these important aspects of the working catalyst is emerging from classic studies and is now extended by in situ TEM and DFT calculations of atomic-scale relationships between structure and catalyst properties and new knowledge about sintering.

Keywords: Steam-reforming; Nickel catalysts; Sulphur poisoning; Sintering; Carbon formation

1. Introduction

Heterogeneous nickel catalysts are commonly used for various industrial processes such as hydrogenation reactions, steam reforming, and methanation. The present paper concentrates on the application of nickel catalysts in steam reforming for the production of hydrogen and synthesis gas. Synthesis gas consists of a mixture of hydrogen, carbon monoxide, and carbon dioxide and is an important intermediate in the industrial syntheses of a wide range of bulk chemicals and fuels [1,2]. Steam reforming was commercialized already in the 1960s and in order to keep on improving the efficiency of the process, it has now to be taken to its limits. Information about the process, the catalyst limits, and catalyst improvements requires ever more sophisticated and detailed information about the catalysts even at the atomic level. The steam-reforming process with its combination of high-pressure hydrocarbons and steam is a challenging environment for the industrial nickel catalysts. In this paper, *four challenges for nickel steam-reforming catalysts*, i.e. activity, sulfur poisoning, carbon formation, and sintering are being discussed. The combination of previous studies and recently obtained atomic-scale insight has resulted in a coherent microscopic picture of the most important aspects of activity, sulfur poisoning, carbon formation, and sintering of nickel catalysts for steam reforming.

2. The steam-reforming process

The main piece of equipment in a steam-reforming unit is the primary reformer, which consists of approximately 10 m long narrow tubes loaded with the nickel catalyst. The tubes are situated in an oven that supplies the thermal energy needed for the reaction and the desired temperature increase. A typical reforming unit is shown in Fig. 1. In more modern units, an adiabatic pre-reformer is situated upstream of the primary reformer to reduce the load and to minimize the risk of sulfur poisoning and carbon formation in the primary reformer [1,2].

The reactions involved in steam reforming of natural gas are described in Table 1.

Steam reforming is strongly endothermic (as seen from the standard enthalpy of reaction) and leads to an expansion of the gas. Steam reforming must therefore ideally be carried out at high temperature, low pressure, and high steam-to-hydrocarbon ratio in order to achieve maximum conversion. The pressures of 20–40 bar typically applied in industrial reforming units are dictated by the high pressures in the synthesis loops, the necessity of high throughput and low pressure drop on one side and the reduced conversion and increasing cost of using high pressures on the other side.

* Tel.: +45 45272365; fax: +45 45272999.
E-mail address: jss@topsoe.dk.

0920-5861/$ – see front matter © 2005 Elsevier B.V. All rights reserved.
doi:10.1016/j.cattod.2005.10.002

Fig. 1. The steam-reforming unit.

3. The four challenges for nickel steam-reforming catalysts

The combination of high temperatures and the presence of hydrocarbons and high-pressure steam creates a severe environment for nickel catalysts, and during operation the nickel steam-reforming catalysts encounter *four challenges*. The challenges are strongly interconnected and are shown in Fig. 2 and briefly described below:

(1) *Activity*: The catalyst must have sufficient activity to equilibrate the reaction mixture in the design catalyst volume. This is especially important in the adiabatic pre-reformer, where the effective activity determines the temperature profile in the reactor and thereby the reactor volume needed to equilibrate the gas mixture.
(2) *Sulfur poisoning*: Even after a thorough desulfurization of the feedstock, sulfur-containing compounds in the feed may reach the nickel catalyst at a ppb level. Sulfur is a strong poison for nickel catalysts and blocks the active nickel sites. The sulfur adsorption capacity of steam-reforming catalysts is therefore an important catalyst parameter.
(3) *Carbon formation*: Carbon formation may increase the pressure drop, crush the catalyst pellets, block the active nickel surface, and even form at the inner perimeter of the reforming tubes resulting in a lower heat transfer. Therefore, the limits for carbon free operation are important for the design and operation.
(4) *Sintering*: Nickel particles in the catalyst may grow during operation. This process is called sintering. Sintering influences the three other catalytic challenges so sintering is important in steam reforming due to the high temperatures and high pressures of steam.

Table 1
Steam-reforming reactions

Reactions	ΔH°_{298} (kJ/mol)[a]
1. $CH_4 + H_2O \rightleftarrows CO + 3H_2$	−206
2. $CO + H_2O \rightleftarrows CO_2 + H_2$	41
3. $C_nH_m + nH_2O \rightarrow nCO + \left(n + \frac{m}{2}\right)H_2$	−1175[b]

[a] Standard state: 298 K and 1 bar.
[b] For n-C_7H_{16}.

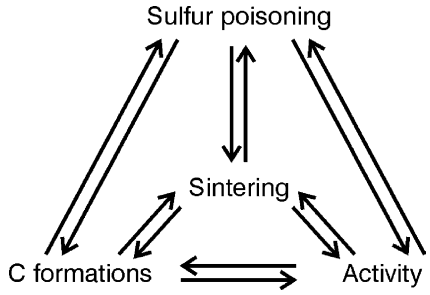

Fig. 2. The four challenges for nickel steam-reforming catalysts.

The four challenges will be discussed in more detail below with the objective of bridging the gap between studies of working catalysts and fundamental knowledge at the atomic level.

4. Activity

In a primary reformer, severe sulfur poisoning or sintering is typically the main reason for low activity resulting in higher tube temperatures and even carbon formation. However, in the adiabatic pre-reformer, the activity is a crucial parameter for the lifetime of a catalyst charge. Many studies of the kinetics of nickel steam-reforming catalysts are reported as summarised in Refs. [2,3]. Many of the kinetic expressions show complicated dependencies on the partial pressures of reactants and products. A simple expression for the kinetics of methane steam reforming over nickel catalysts was recently proposed by Wei and Iglesia [3]. They found that the activity at 600–700 °C only depends on the partial pressure of methane implying that abstraction of the first hydrogen atom is the rate-determining step. This conclusion was supported by activity measurements using CH_4/CD_4 isotopomers [3]. The active sites were found to be free of any

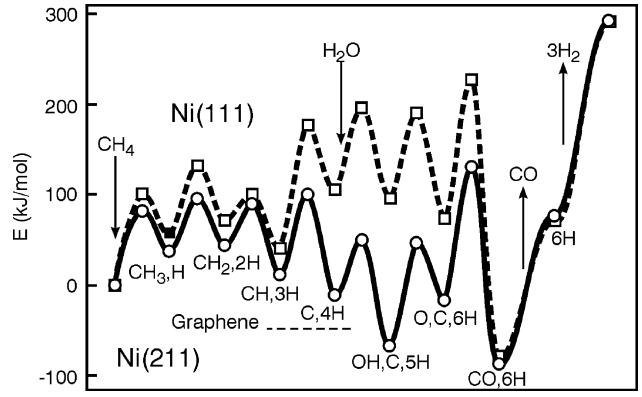

Fig. 3. Calculated energies along the reaction path for steam reforming on Ni(1 1 1) and Ni(2 1 1) surfaces [4].

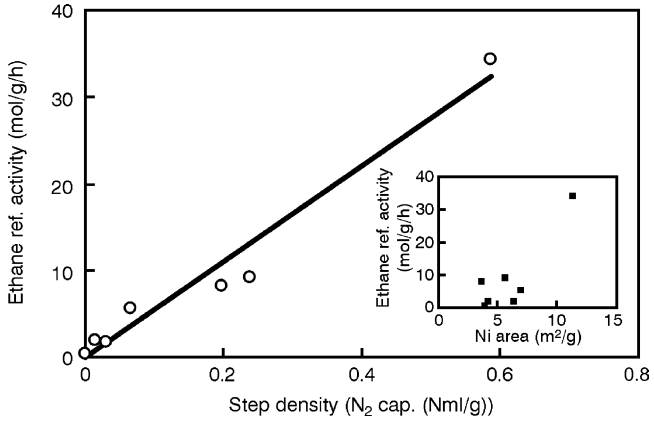

Fig. 4. Rate of reforming of ethane at 500 °C (H_2O:C_2:H_2 = 8:1.25:1) over Ni/Al_2O_3 catalysts [5] plotted as a function of the N_2 adsorption capacity. The insert shows the activity plotted as a function of the Ni area. The three catalysts with lowest activities are potassium promoted.

reaction intermediates. At lower temperatures and higher pressures this may not necessarily be the case and therefore more complicated kinetic expressions will most likely be obtained at other experimental conditions [2,3].

The nature of the active site is still debated. Several theoretical and experimental studies indicate that step sites are the main active sites. Bengaard et al. [4] determined the energy path for methane reforming at terrace and step sites by Density Functional Theory Calculations (see Fig. 3). The lowest energy barriers are encountered at the step sites suggesting that these sites dominate the rate of reforming. Important species like H atoms and CO molecules, which may block the surface, have similar adsorption energies at steps and terraces indicating similar coverages of these species at the two types of sites. Contrary to this, carbon atoms and OH radicals adsorb considerably stronger at steps than at terraces.

The importance of steps for the activity of reforming catalysts is also supported by the experimental data in Fig. 4. There is a good correlation between reaction rate and step density as determined by N_2 adsorption [6]. The correlation between activity and nickel surface area is much less satisfactory as seen at the inset in Fig. 4. The data in Fig. 4 indicate that reaction at step sites dominates the overall activity. Interestingly, potassium promotion decreases both the activity and the step density while it hardly affects the nickel area [1,2]. This is in agreement with DFT calculations, which shows that potassium is more strongly bonded to step than to terrace sites [4].

The nickel step density may depend on the nickel particle size. By geometrical considerations, van Hardeveld and van Montfoort [7] described quantitatively the strong decrease in the number of step sites per surface area with increasing particle size. Wei and Iglesia [3] found that the steam-reforming activity per unit metal surface area increases with dispersion for noble metals, but the data are less certain for nickel catalysts. Contrary to this observation, the area specific activity data in Table 2 for two catalysts with different nickel particle size, but similar nickel surface area show no increase with dispersion.

Direct measurements of the area specific number of step sites (N_2 chemisorption) at non-alkali promoted nickel catalysts plotted as a function of nickel particle diameters are presented in Fig. 5 [5]. Note that the N_2 adsorption capacity for the catalyst with the largest particle diameter is small (5 N ml/kg) and hence very uncertain. There is large scatter and no obvious de- or increasing trends in the data.

No dependence on particle size is observed in the area specific activity and step density in the data in Table 2 and Fig. 5. It may be speculated that this is due to the low step energy of nickel (16 kJ/mol for Ni(2 1 1) relative to Ni(1 1 1) [8]). Considering the dynamics of metal surfaces at elevated temperatures, it seems reasonable that steps and terraces are constantly formed and removed during operation. This "steady state" between steps and terraces may dominate the number of step sites for large nickel particles, while the number of steps per nickel area for small particles is more likely to be dominated by the size of the particles according to the work of van Hardeveld and van Montfoort [7]. In this scenario, the area specific step density and activity may therefore depend on the average nickel particle diameter for small but not for large particles.

To conclude, Figs. 3 and 4 indicate that steam-reforming activities of nickel catalysts depend on the number of step sites.

Table 2
Comparison of activities of two nickel catalysts with equal nickel surface areas but different nickel particle sizes [4]

Catalyst	d_{Ni} (S-chemisorption) (nm)	Dispersion (%)	Nickel surface area (S-chemisorption) ($m^2\ g^{-1}$)	Activity[a] (mol/g/h)	Activity/nickel surface area (mol/m^2/h)
0.92 wt.% Ni/$MgAl_2O_4$	7	14.4	1.00	0.26	0.26
15 wt.% Ni/$MgAl_2O_4$	102	0.99	0.90	0.29	0.32

[a] Activity at 500 °C in a gas mixture containing 19% CH_4, 7% H_2, and 74% H_2O at ambient pressure.

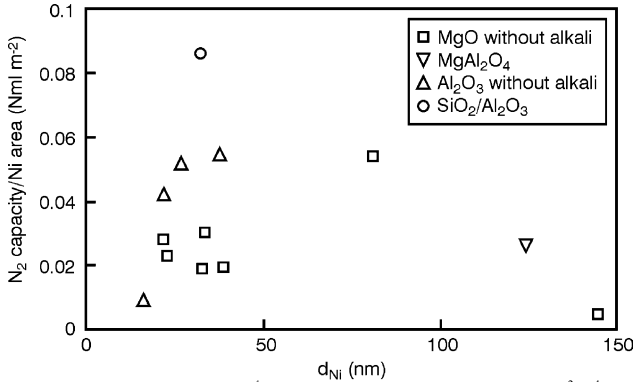

Fig. 5. N_2 adsorption capacity (N ml g^{-1}) divided by the nickel surface area (m^2 g^{-1}) plotted as a function of nickel particle diameter. The data were obtained from Ref. [5]. See text for details.

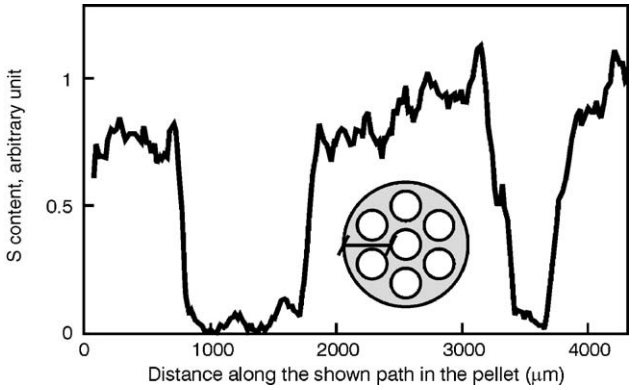

Fig. 6. Sulfur uptake profile of a severely sulfur-poisoned seven-hole reforming catalyst.

The data in Table 2 and Fig. 5 suggest that the surface concentration of step sites and area specific activity do not depend on dispersion at least for large particle sizes ($\gtrsim$7 nm). To prove these two points explicitly, more work is needed. It is important to note that in any case, an increase in the nickel particle size decreases the activity of a steam-reforming catalyst. Hence, activity and sintering is strongly connected, since nickel particle growth via sintering reduces catalyst activity.

5. Sulfur poisoning

Sulfur is a severe and common poison for nickel steam-reforming catalysts as a sulfur-poisoned nickel catalyst has essentially no activity below 700 °C [1,2]. All sulfur-containing compounds in the feed are converted into hydrogen sulfide at reforming conditions. The sulfur atom in hydrogen sulfide adsorbs strongly at the nickel surface:

$$H_2S + Ni_{surface} \rightleftarrows Ni_{surface}{-}S + H_2$$

The S:Ni surface stoichiometry is approximately 0.5, which corresponds to a sulfur uptake of 440 ppm S (weight basis) per m^2 g^{-1} of nickel [1,2]. Formation of nickel sulfide is only observed at much higher sulfur levels than normally experienced in a reformer. The maximum sulfur uptake in a reformer is therefore proportional to the nickel surface area and is then connected to the extent of sintering of the catalyst.

The H_2S equilibrium pressure is extremely low at moderate sulfur coverages $\left(\left(\frac{P_{H_2S}}{P_{H_2}}\right)_{eq} \sim 2 \times 10^{-13}, \theta_s = 0.5, 450\,^{\circ}C\right)$. Consequently, sulfur in the feed will be almost quantitatively withheld until saturation. The low H_2S equilibrium pressure is also reflected in the radial sulfur profile in the catalyst pellet, as illustrated in Fig. 6, which shows a sharp sulfur front in the pellet. The uptake forms a shell with a thickness of about 800 μm. Only the volumes furthest away from the outer surface and the holes are unpoisoned. The overall effect of sulfur poisoning is determined by the sulfur adsorption capacity, i.e. the nickel surface area and the shape of the catalyst pellets. The sulfur uptake in a more advanced catalyst shape is faster than in a cylinder resulting in sulfur poisoning of a smaller part of the catalyst bed. Furthermore, the pressure drop is lower for shapes with internal holes.

6. Carbon formation

Steam reforming of hydrocarbons involves a risk of carbon deposition. Carbon deposition may reduce the performance of the catalyst charge in several ways, and it may eventually have to be replaced. Three types of carbon have been observed in a reformer: pyrolytic, encapsulating and whisker carbon as imaged by electron microscopy in Fig. 7.

Pyrolytic carbon (Fig. 7A) is formed by exposure of higher hydrocarbons to high temperatures. Higher hydrocarbons may reach high temperatures in the reformer as a result of low activity for example due to sulfur poisoning or sintering of the catalyst in the colder upper parts of the reactor tubes. The result may be ‘‘hot bands’’ between one-third and halfway down the reactor tubes.

Encapsulating carbon (gum) (Fig. 7B) may be formed during reforming of heavy hydrocarbon feeds with a high content of aromatic compounds. The rate of gum formation is enhanced by low temperatures and high final boiling point of the hydrocarbon mixture. Encapsulating carbon consists of a thin CH_x film or a few layers of graphite covering the nickel particles as illustrated in Fig. 7B resulting in loss of activity and hence deactivation of the catalyst bed. Deactivation of a pre-reformer due to gum is observed as a drift of the temperature profile in the catalyst bed with no increase in the pressure drop. Gum formation may be difficult to distinguish from sulfur poisoning.

Whisker carbon is the most destructive form of carbon formed in steam reforming over nickel catalysts. A thermodynamic limit exists for equilibrated gas. Carbon may also be formed kinetically from higher hydrocarbons if the ratio of steam to higher hydrocarbons is too low. Carbon whiskers grow by the reaction of hydrocarbons or CO at one side of the nickel particle and nucleation of graphitic carbon as a carbon whisker on the other side of the nickel particle, as shown schematically in Fig. 8 and imaged in Fig. 7C.

DFT calculations and in situ electron microscopy [4,9] have recently shed new light on the formation and growth of carbon

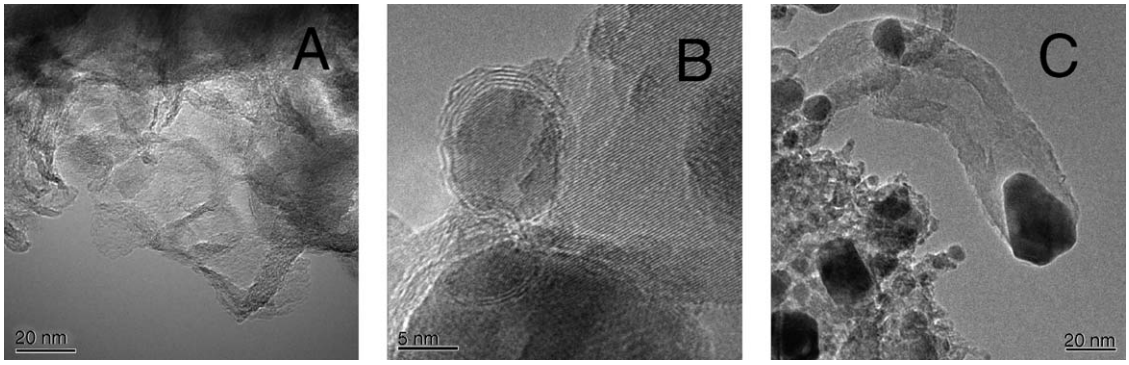

Fig. 7. Electron microscopy images (Philips CM200 FEG TEM) of pyrolytic carbon on a $MgAl_2O_4$ carrier (A), encapsulating carbon (B), and whisker carbon (C) on $Ni/MgAl_2O_4$ reforming catalysts.

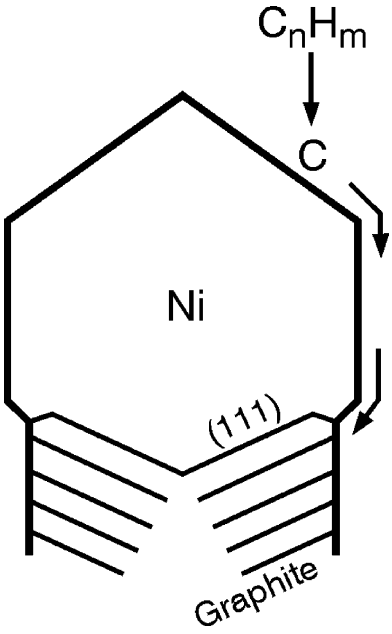

Fig. 8. Schematic illustration of the process by which carbon whiskers are formed catalytically at the nickel particle during steam reforming.

whiskers. It is clear from the energy diagram in Fig. 3 that adsorbed atomic carbon is much more stable at nickel steps than at nickel terraces. Consequently, steps are better nucleation sites for carbon than terraces. When carbon atoms cover step sites, a graphene layer (single graphite layer) can grow from the step, as illustrated in Fig. 9A. It is interesting to compare the energy of carbon in a graphene layer at the Ni(1 1 1) surface (dashed line in Fig. 3) to that of carbon at a Ni(2 1 1) step (see Fig. 3). The energy of carbon in a graphene layer is below the energy of the most stable form of surface-adsorbed carbon (at the step), hence there is a driving force for graphene formation. After a graphene island has nucleated, the growth may continue by surface or bulk transport of carbon atoms or carbon-containing fragments to the island. Graphene may eventually cover the whole crystallite, encapsulating the nickel particle. In this situation, gum is formed and carbon formation ceases. Alternatively, new layers may nucleate below the first graphene layer and grow by addition of carbon atoms. This growth is accompanied by surface transport of nickel to the free nickel surface resulting in growth of a carbon whisker from the nickel particle [9]. The transport route of carbon has been debated, but recently DFT calculations strongly indicated that transport of carbon proceeds via the nickel surface and the nickel–graphite interface [9].

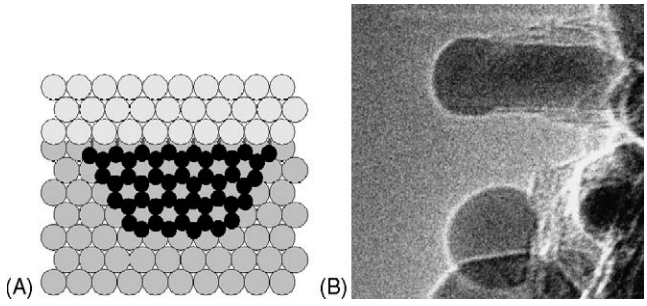

Fig. 9. (A) Illustration of a graphene island nucleated from a Ni(2 1 1) step at a Ni(1 1 1) surface [4]. (B) ''Lift off'' for a nickel particle from the carrier due to carbon formation [9].

The coherent picture of carbon formation is verified by in situ electron microscopy films of the initial carbon formation. A snapshot of the carbon formation just after start of formation is shown in Fig. 9B. The image shows that the graphene layers are terminated at one end by nickel step sites in accordance with the low step energy for carbon in Fig. 3. This observation combined with the data in Figs. 3 and 4 indicate that the availability of step sites is important both to obtain a high turnover rate and for the formation of whisker carbon. Interestingly, DFT calculations suggest that species such as potassium, sulfur, and gold are preferentially located at step sites; sulfur and gold are 48 and 36 kJ/mol more stable at steps than at terrace sites, and potassium as -K-O-K-O- rows along nickel steps are 75 kJ/mol more stable than at terraces [2,4]. Thus, a major carbon-preventing effect of these promoters and poisons is to block the nickel steps and hence remove the nucleation sites for graphite formation.

7. Sintering

Sintering describes a process in heterogeneous catalysts where small particles grow in size. This development is driven

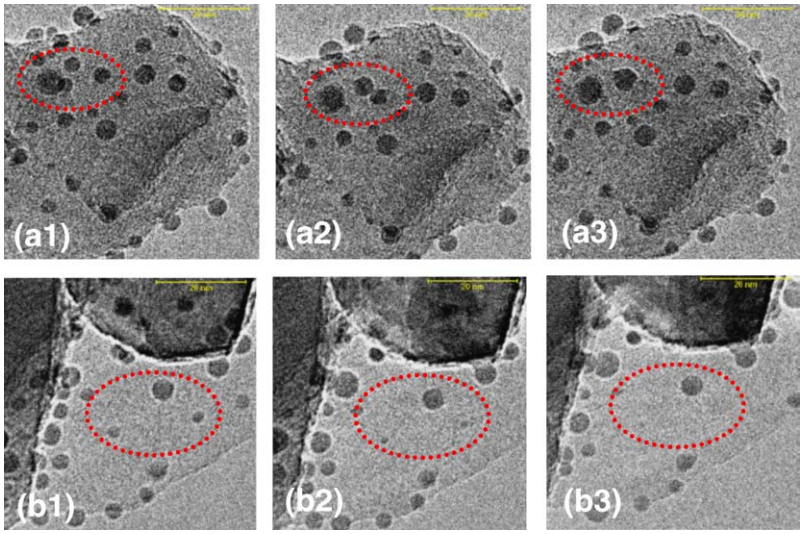

Fig. 10. A series of electron microscopy images (Philips CM300 FEG TEM) of a Ni/$MgAl_2O_4$ reforming catalyst: sequence (a) illustrates the particle migration and coalescence sintering mechanisms. Sequence (b) illustrates the Ostwald ripening mechanism. The conditions were 706 °C and 3.1 mbar H_2. Relative times were 0 s (a1), 44.5 s (a2), and 65 s (a3) and 0 s (b1), 41 s (b2), and 44.5 s (b3).

by a reduction in the total surface energy. Sintering of nickel steam-reforming catalysts influences the three other catalytic challenges for these catalysts. The coking limits are affected by the nickel particle size, the nickel surface area determines the sulfur capacity, and the activity is related to nickel particle size [1,2]. To model an industrial reformer with regard to activity, sulfur poisoning, and coking limits, it is therefore necessary to estimate the nickel surface area as a function of time, temperature, feed gas composition, chemical composition including promoters, and extent of poisoning.

Two mechanisms for the metal particle growth have been proposed: (i) particle migration, where entire crystallites migrate over the support followed by coalescence, (ii) Ostwald ripening (atom migration or vapor transport), where metal transport species emitted from one crystallite, migrate over the support or via the (gas) phase and are captured by another crystallite. The two fundamental sintering mechanisms are illustrated by electron microscopy sequences in Fig. 10.

The first aim in this section is to present a simple model for sintering via particle migration and coalescence and compare the results of such a model with experimentally obtained data for nickel steam-reforming catalysts [10–12]. The second aim is to give a reason for the increase in the rate of sintering observed at high temperatures, i.e. it is proposed here that this observation is related to a change in the sintering mechanism from particle migration to atom migration.

To derive a model for sintering via particle migration and coalescence, it is necessary to calculate the diffusivity of the metal particles. At the surface of a nickel particle, nickel transport species as for example nickel adatoms move randomly. Transport of a nickel atom from one side of a particle to the other, results in a translational motion of the center of the particle (see Fig. 11). Therefore, surface transport of nickel atoms at nickel particles results in particle migration.

Gruber [13] derived an expression for the diffusion of gas bubbles in metals, which may also be used to describe the diffusion of metal particles on ceramic carriers [14]. The equation links the diffusion constant of metal particles, D_{particle}, to the diffusion constant of metal atoms at the surface of metal particles, D_{atom}:

$$D_{\text{particle}} = 4.81 D_{\text{atom}} \left(\frac{a_0}{d_{\text{particle}}} \right)^4$$

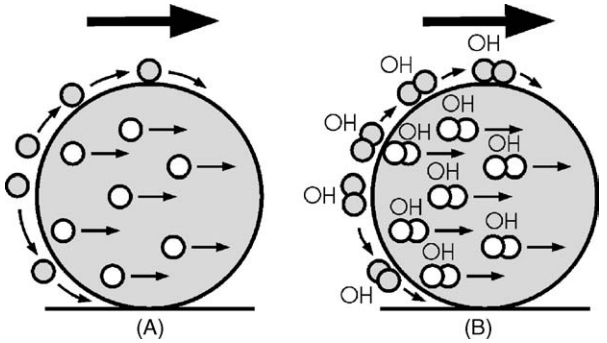

Fig. 11. Illustrations of the mechanisms for particle movement mediated by adatoms (A) or Ni_2OH complexes (B).

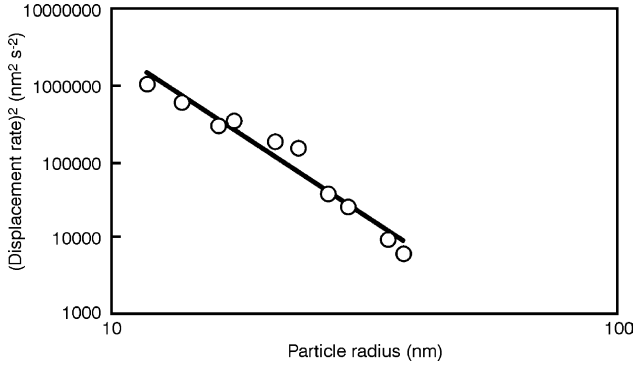

Fig. 12. The square of the displacement rate for Fe particles at carbon at 740 °C and 6.6 mbar CO as a function particle radius [15].

where a_0 is the inter-atomic distance and $d_{particle}$ is the particle diameter. Experimental evidence exists for this strong dependence of the diffusivity of metal particles on the particle diameter. For example, the diffusivity of iron supported at carbon in an atmosphere of 6.6 mbar of CO at 740 °C was studied by Baker et al. [15]. The squares of the displacement rates plotted as a function of particle radii in the range 12–38 nm are given in Fig. 12. The square of the displacement rate is proportional to the particle diameter in the power of −4.4, which is in reasonable agreement with the power of −4 predicted by Gruber [13]. Furthermore, Yak et al. [16] found recently that the expression $D_{particle} = \text{const.} \times d_{particle}^{-4}$ predicts the growth of Pd particles at TiO_2(1 1 0) well. It therefore seems reasonable to use the formula above connecting $D_{particle}$ and D_{atom} when adatoms dominate the surface transport at metal particles.

It is well established that sintering of metal catalysts depends on the partial pressure of steam [11,12,17]. However, the expression above does not include any dependence of $D_{particle}$ on the atmosphere over the catalyst. Consequently, $D_{particle}$ has to be modified to include the observed dependencies of the atmosphere over nickel catalysts. Interestingly, it was shown recently that adsorbants may induce increased sintering via the so-called ''skyhook'' effect, where increased surface transport are mediated by formation of metal adsorbant complexes with either low formation energy or increased diffusivities [18–21]. For nickel steam-reforming catalysts, DFT calculations show that the combined energy of formation and diffusion for Ni_2–OH complexes at Ni(1 1 1) is 40 kJ/mol lower than that for nickel adatoms, strongly indicating that the former species are dominating the surface transport of nickel at nickel surfaces when steam is present in the atmosphere [12]. The particle diffusion constant in the presence of steam (and hydrogen) is given by [12]:

$$D_{particle}^{OH\text{-}dimer} = 9.62 D_{OH\text{-}dimer} \left(\frac{a_0^4}{d_{particle}^4} \right) K_{OH\text{-}dimer} \frac{P_{H_2O}}{P_{H_2}^{0.5}}$$

where $D_{OH\text{-}dimer}$ and $K_{OH\text{-}dimer}$ are the diffusion coefficient of and the equilibrium constant for the formation of a Ni_2–OH complex at nickel. Assuming that the Ni_2–OH complex, steam and hydrogen are in equilibrium, that the carrier is only characterized by a surface area, and that the particle size distribution is log normal with constant standard deviation as often observed in sintering studies [22], it is possible to derive an approximate expression for the development of the average particle diameter, $\overline{d}_{Ni}$, as a function of a series of parameters [11,12]:

$$\frac{\overline{d}_{Ni}}{\overline{d}_{Ni,0}} = \left(\text{const.} \frac{K_{OH\text{-}dimer} D_{OH\text{-}dimer} X_{Ni} \tau}{(1 - X_{Ni}) A_{car} \overline{d}_{Ni,0}^7} \left(\frac{P_{H_2O}}{P_{H_2}^{0.5}} \right) + 1 \right)^{1/7}$$

where X_{Ni} is the weight fraction of nickel, A_{car} the surface area of the carrier per gram of carrier, τ the sintering time, $\overline{d}_{Ni,0}$ the average nickel particle diameter of the fresh sample, P_{H_2O} and P_{H_2} the partial pressures of steam and hydrogen, and const. $K_{OH\text{-}dimer} D_{OH\text{-}dimer}$ is a temperature-dependent constant, which may for example be determined experimentally.

Model	Experiment
$d_{Ni} \propto X_{Ni}^{0.14}$	$d_{Ni} \propto X_{Ni}^{0.14}$
$d_{Ni} \propto A_{carrier}^{-0.14}$	$d_{Ni} \propto A_{carrier}^{-0.3}$
$d_{Ni} \propto P_{H2}^{-0.07}$	$d_{Ni} \propto P_{H2}^{-0.07}$
$d_{Ni} \propto t^{0.14}$	$d_{Ni} \propto t^{0.14}$
$d_{Ni} \propto \exp[\sim 20\text{kJ/mol/RT}]$	$d_{Ni} \propto \exp[\sim 20\text{kJ/mol/RT}]$

Fig. 13. Comparison of the dependencies of the average nickel particle diameter on various parameters obtained by a model and experimentally [11,12] ($T \leq 581$ °C).

According to the equation above, the sensitivity of the average particle diameter on the various parameters will vary with time. However, for severely sintered samples, $\text{const.} \frac{K_{OH\text{-}dimer} D_{OH\text{-}dimer} X_{Ni} \tau}{(1-X_{Ni}) A_{car} \overline{d}_{Ni,0}^7} \left(\frac{P_{H_2O}}{P_{H_2}^{0.5}} \right) \gg 1$ and the dependencies of the average particle diameters on various parameters obtained from the model are given in the first column in Fig. 13.

The modeled dependencies of $\overline{d}_{Ni}$ on various parameters may be compared to the dependencies obtained experimentally. For that purpose, a series of nickel catalysts with various nickel loadings supported on $MgAl_2O_4$ carriers were aged for 664–700 h at 500 °C, H_2O:H_2 = 10:1 and 31 bar total pressure. Furthermore, a 22 wt.% Ni/$MgAl_2O_4$ catalyst was aged for 700 h at various temperatures in the range of 483–682 °C in H_2O:H_2 = 10:1 and at 31 bar total pressure and in H_2O:H_2 = 2.5:1 at 40 bar total pressure [11,12]. The average nickel particle diameters were determined by sulfur chemisorption according to the method described previously [1,2].

The experimentally determined dependencies (for $T \leq 581$ °C) of $\overline{d}_{Ni}$ on various parameters are given in the right column in Fig. 13. Clearly, there is good correspondence between the experimental and the modelled dependencies of $\overline{d}_{Ni}$ giving credit to the sintering model. The experimentally determined effect of the carrier surface area is somewhat stronger than that predicted by the model. However, this may not be too surprising considering that the carrier in the model is only characterised by the total carrier surface area.

Sintering in H_2O/H_2 atmospheres at temperatures above approximately 600 °C results in an increase in the rate of sintering as seen in Fig. 14, where $\frac{\overline{d}_{Ni}}{\overline{d}_{Ni,0}}$ is plotted as a function of the temperature. According to the data in Fig. 14, the average

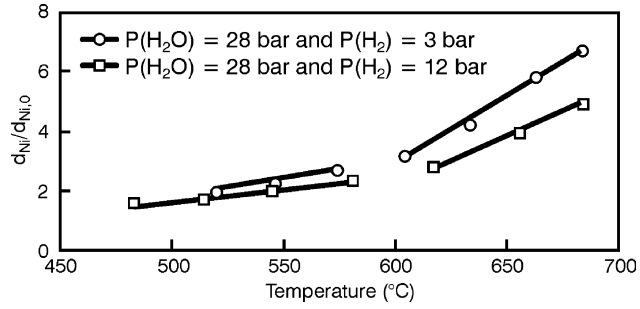

Fig. 14. Relative average nickel particle diameter in a 22 wt.% Ni/$MgAl_2O_4$ catalyst after sintering for 700 h plotted as a function of the sintering temperature [11,12].

nickel particle diameter grows considerably faster with temperature above than below 600 °C. Furthermore, the dependence on atmosphere, for example the effect of hydrogen partial pressure, is stronger above 600 °C. These variations with temperature may be interpreted as a change in the sintering mechanism. Loss of nickel would also result in low sulfur chemisorption and hence high d_{Ni}. However, in order to explain the additional loss of nickel surface area at high temperatures compared to at low temperatures, >90% of the nickel should be lost for example by reaction with the carrier at 684 °C, which was not observed. A reasonable hypothesis is therefore that the additional loss of nickel surface area above 600 °C is due to a change in the sintering mechanism from particle migration and coalescence to Ostwald ripening via atom migration at the support. This mechanism change also seems reasonable considering that it is expected that the energy involved in creating and moving nickel transport species at the surface of nickel particles is lower than the energy involved in nickel transport at a carrier.

Two limiting regimes exist for migration of nickel transport species at the carrier [14]: (i) *Interface* controlled coarsening, where metal diffusion at the carrier is fast and the rate of sintering is therefore determined by the flux across the edge of the particle. (ii) *Diffusion* controlled coarsening, where diffusion across the carrier is the rate-determining step. In the following, only *interface* controlled coarsening will be considered for two reasons. The energy barrier across the edge of the particle is expected to be much higher than the diffusion barrier at the surface of the carrier. Furthermore, the time dependence of the sintering fits the *interfaced* controlled Ostwald ripening well [23].

Interestingly, the data in Fig. 14 obtained after sintering above 600 °C show a large decrease in the rate of sintering upon an increase in the partial pressure of hydrogen by a factor of 4. This effect is included in the model for *interfaced* controlled Ostwald ripening by assuming that OH bonded nickel dimers are dominating the nickel transport at both nickel and carrier surfaces. Consequently, the expressions presented by Wynblatt and Gjostein [14] have to be modified and the new equation for the time dependence of the average nickel particle diameter, including the environmental dependence, is given by:

$$\frac{\overline{d}_{Ni}}{\overline{d}_{Ni,0}} = \left(\frac{Kt}{\overline{d}^3_{Ni,0}} \left(\frac{P_{H_2O}}{P^{0.5}_{H_2}} \right) + 1 \right)^{1/3}$$

where K, among other parameters, contains the equilibrium constant and diffusion barrier for formation and diffusion of the Ni_2–OH complex at the carrier, respectively.

The experimentally determined dependence of the rate of sintering at 620 °C on the partial pressure of hydrogen may be obtained from a fit to the data (>600 °C) in Fig. 14. The effect of ageing in $P_{H_2O} = 28$ bar and $P_{H_2} = 3$ bar compared to $P_{H_2O} = 28$ bar and $P_{H_2} = 12$ bar is an increase in the value of $\frac{K}{d^3_{Ni,0}} \left(\frac{P_{H_2O}}{P^{0.5}_{H_2}} \right)$ of 2.26 compared to the value of 2 obtained theoretically. The good agreement between experiments and theory gives some credit to the interpretation of the observed increase in the rate of sintering above 600 °C presented here.

8. Conclusion

Reforming has been used commercially for more than 40 years and is now taken to its limits in order to improve the efficiency of the process. More detailed and fundamental knowledge of nickel catalysts is therefore needed. As demonstrated here, a broad knowledge base has to a large extent appeared in the classic studies and is now extended by in situ TEM and DFT studies of atomic-scale relationships between structure and catalyst properties and new knowledge about sintering. Many observations of reforming catalysts at industrial conditions can now be rationalised from more fundamental studies. Even though many details are still unknown, a coherent picture of the most important aspects of the use of nickel catalysts in steam reforming has emerged.

References

[1] J.R. Rostrup-Nielsen, in: J.R. Anderson, M. Boudart (Eds.), Catalysis, Science and Technology, vol. 5, Springer-Verlag, Berlin, 1984 (Chapter 1).
[2] J.R. Rostrup-Nielsen, J. Sehested, J.K. Nørskov, Adv. Catal. 47 (2002) 65.
[3] J. Wei, E. Iglesia, J. Catal. 224 (2004) 370.
[4] H.S. Bengaard, J.K. Nørskov, J. Sehested, B.S. Clausen, L.P. Nielsen, A.M. Molenbroek, J.R. Rostrup-Nielsen, J. Catal. 209 (2002) 365.
[5] J.R. Rostrup-Nielsen, Steam Reforming Catalysts, Danish Technical Press, Copenhagen, 1975.
[6] R. van Hardeveld, A. van Montfoort, Surf. Sci. 17 (1969) 90.
[7] R. van Hardeveld, A. van Montfoort, Surf. Sci. 4 (1966) 396.
[8] H.S. Bengaard, Ph.D. Thesis, Danish Technical University, 2001.
[9] S. Helveg, C. López-Cartes, J. Sehested, P.L. Hansen, B.S. Clausen, J.R. Rostrup-Nielsen, F. Abild-Pedersen, J.K. Nørskov, Nature 427 (2004) 426.
[10] J. Sehested, A. Carlson, T.V.W. Janssens, P.L. Hansen, A.K. Datye, J. Catal. 197 (2001) 200.
[11] J. Sehested, J. Catal. 217 (2003) 417.
[12] J. Sehested, J.A.P. Gelten, I.N. Remediakis, H. Bengaard, J.K. Nørskov, J. Catal. 223 (2004) 432.
[13] E.E. Gruber, J. Appl. Phys. 38 (1967) 243.
[14] P. Wynblatt, N.A. Gjostein, Prog. Solid State Chem. 9 (1975) 21.
[15] R.T.K. Baker, P.S. Harris, R.B. Thomas, Surf. Sci. 46 (1974) 311.
[16] M.J.J. Yak, C. Konstapel, A. van Kreuningen, J. Verboeven, J.W.M. Frenken, Surf. Sci. 457 (2000) 295.
[17] C.H. Bartholomew, Appl. Catal. A 107 (1993) 1.
[18] R. Stumpf, Phys. Rev. B 53 (1996) R4253–R4256.
[19] S. Horch, H.T. Lorensen, S. Helveg, E. Lægsgaard, I. Stensgaard, K.W. Jacobsen, J.K. Nørskov, F. Besenbacher, Nature 398 (1999) 134.
[20] P.J. Feibelman, Phys. Rev. Lett. 85 (2000) 606.
[21] W.L. Ling, N.C. Bartelt, K. Pohl, J. de la Figuera, R.Q. Hwang, K.F. McCarty, Phys. Rev. Lett. 93 (2004) 166101.
[22] C.G. Granqvist, R.A. Buhrman, Appl. Phys. 47 (1976) 2200.
[23] J. Sehested, S. Helveg, in preparation.